

**Longitudinal acoustic and higher-energy excitations in the liquid phase-change material  $\text{Ge}_2\text{Sb}_2\text{Te}_5$** M. Inui<sup>1,\*</sup>, Y. Kajihara<sup>1</sup>, S. Hosokawa<sup>2,†</sup>, A. Chiba<sup>3</sup>, Y. Nakajima<sup>2</sup>, K. Matsuda<sup>2</sup>, Y. Tsuchiya<sup>4</sup>, J. R. Stellhorn<sup>1</sup>, T. Hagiya<sup>5,‡</sup>, H. Uchiyama<sup>6</sup>, S. Tsutsui<sup>6</sup> and A. Q. R. Baron<sup>7</sup><sup>1</sup>*Graduate School of Advanced Science and Engineering, Hiroshima University, Higashi-Hiroshima 739-8521, Japan*<sup>2</sup>*Department of Physics, Kumamoto University, Kumamoto 860-8555, Japan*<sup>3</sup>*Department of Physics, Keio University, Yokohama 223-8522, Japan*<sup>4</sup>*Niigata University, Niigata 950-2181, Japan*<sup>5</sup>*Graduate School of Science, Kyoto University, Kyoto 606-8502, Japan*<sup>6</sup>*Japan Synchrotron Radiation Research Institute (JASRI), Sayo, Hyogo 679-5198, Japan*<sup>7</sup>*Materials Dynamics Laboratory, RIKEN Spring-8 Center, Sayo, Hyogo 679-5148, Japan*

(Received 5 August 2020; revised 30 June 2021; accepted 6 July 2021; published 16 August 2021)

The dynamic structure factor  $S(Q, E)$  of liquid  $\text{Ge}_2\text{Sb}_2\text{Te}_5$  has been obtained by inelastic x-ray scattering, where  $Q$  and  $E$  are momentum and energy transfer, respectively. The dispersion curve of the longitudinal acoustic excitation energy exhibits flat-topped  $Q$  dependence similarly to that in liquid  $\text{GeTe}$  and liquid  $\text{Bi}$ , where the local structure is modulated by Peierls distortion. The flat-topped energy in liquid  $\text{Ge}_2\text{Sb}_2\text{Te}_5$  is split into low and high energy parts arising from Sb-Te and Ge-Te correlations, respectively. Furthermore, the high energy part depends on  $Q$  like an optical mode with decreasing  $Q$  to zero, and it approaches the vibrational energy of fourfold coordinated Ge atoms with octahedral configurations. The result indicates that a majority of Ge in the liquid stays in octahedral order as predicted by first-principles molecular dynamics simulations.

DOI: [10.1103/PhysRevB.104.064202](https://doi.org/10.1103/PhysRevB.104.064202)**I. INTRODUCTION**

Fast phase-change materials (PCMs) have been intensively investigated for the last two decades since the fast phase-change phenomena between crystalline and amorphous states were utilized in nonvolatile memory [1]. PCMs for memory devices show strong optical contrast between the crystalline and amorphous states and its origin has been related to the difference in bonding properties between them [2–5].

From those studies it was pointed out that Peierls distortion [6] and charge transfer [7] play central roles in PCMs. Here we focus on Peierls distortion. Peierls described that the one-dimensional regular lattice of a monovalent metal is unstable for dimerization with a gap at the zone boundary in the electronic states [8]. The essentially same idea had been proposed by Jones [9] to understand the distorted rocksalt (A7) structure in Bi with five valence electrons, 20 years prior to Peierls [10]. Jones discussed the energy gain with a distortion, considering an energy gap appearing in the three-dimensional momentum space. By replacing the energy surface in the three-dimensional space with the zone boundary, Peierls suggested a model easily understood. Hence, the phenomenon is now called a Peierls instability or Peierls distortion. A Peierls instability occurs not only in crystals but also in liquids [6,11]. A neutron diffraction (ND) study revealed that liquid

$\text{Ge}_2\text{Sb}_2\text{Te}_5$  belongs to the family of Peierls distortion [12], by which the nearest neighbor (NN) coordination number of approximately three and the alternation of shorter and longer bonds like the distorted rocksalt structure are stabilized. Later the profile of the total structure factor  $S(Q)$  of several liquids including liquid  $\text{Ge}_2\text{Sb}_2\text{Te}_5$  was discussed as indicative of the octahedral local order with Peierls distortion [13].

In the memory device, an amorphous bit is formed by rapid quenching a liquid spot made by laser beam irradiation. To understand fast crystallization in PCMs, many structural studies on amorphous  $\text{Ge}_2\text{Sb}_2\text{Te}_5$  have been carried out using experimental techniques with reverse Monte Carlo (RMC) modeling [14–20], and also using first-principles molecular dynamics (FPMD) simulations [21–25]. Later, the partial structure factors of amorphous  $\text{Ge}_2\text{Sb}_2\text{Te}_5$  were experimentally obtained by RMC [15–18] and new techniques were applied to investigate the amorphous structure [19,20].

It is of great importance to understand fast crystallization from the amorphous state at high temperature in PCMs. Fragile behavior of liquid viscosity in PCMs obtained by thermodynamic investigations [26] has been discussed to contribute to the stability of the amorphous state at the ambient temperature and fast crystallization in the supercooled liquid state at high temperature. From FPMD results, it was pointed out that flexible structural units and weak chemical bonds arising from lone pair orbitals make important contribution to fast crystallization [27]. FPMD simulations on amorphous  $\text{Ge}_2\text{Sb}_2\text{Te}_5$  at high temperatures below the melting point have been carried out on a nanosecond timescale by several research groups [28–32]. These studies suggest that fourfold rings (ABAB squares where A: Ge and Sb; B: Te) play a central role for nucleation as previously pointed out [14,21].

\*masinui@hiroshima-u.ac.jp

†Present address: Institute of Industrial Nanomaterials, Kumamoto University, Kumamoto 860-8555, Japan.

‡Present address: Metal Powder Technology Department, Sanyo Special Steel Co., Ltd., Himeji, Hyogo 672-8677, Japan.

As the dominance of Ge-Sb-Te alloys applied to PCMs, it was addressed that the similarity of *s*- and *p*-valence orbitals in a spatial distribution among Ge, Sb, and Te and the metastable crystalline structure [33] play crucial roles [10].

As a prototype of  $\text{Ge}_2\text{Sb}_2\text{Te}_5$ , it was introduced the phase transition of  $\alpha$ -GeTe with the A7 structure into metastable  $\beta$ -GeTe with the rocksalt structure at high temperature. On melting, GeTe is again transformed into the octahedral liquid with Peierls distortion and the distorted local structure is smeared out at higher temperatures [6]. Hence Peierls distortion appears a key property in the solid and liquid states. New knowledge on liquid  $\text{Ge}_2\text{Sb}_2\text{Te}_5$  must be useful to understand the mechanism of fast crystallization in PCMs.

Besides ND studies [12,13], structural studies on liquid  $\text{Ge}_2\text{Sb}_2\text{Te}_5$  are not so many. An x-ray absorption fine structure (XAFS) study indicated similarity in the local structure between amorphous and liquid  $\text{Ge}_2\text{Sb}_2\text{Te}_5$  [34]. Atomic dynamics in liquid  $\text{Ge}_2\text{Sb}_2\text{Te}_5$  was studied by inelastic neutron scattering (INS) and the vibrational density of states (VDOS) was discussed [35,36]. FPMD simulations also revealed dynamical properties in liquid  $\text{Ge}_2\text{Sb}_2\text{Te}_5$  [21,22,25,32,36,37]. In addition to these studies, information obtained from the dynamic structure factor  $S(Q, E)$ , where  $Q$  and  $E$  are momentum and energy transfer, respectively, is expected to make important contribution to understanding atomic dynamics and fast crystallization in liquid  $\text{Ge}_2\text{Sb}_2\text{Te}_5$ .

So far we have measured  $S(Q, E)$  of liquid GeTe [38] and Bi [39] by inelastic x-ray scattering (IXS), and discussed atomic dynamics in these liquids. Previously, Bi and Sb were not classified as the liquids with Peierls distortion because of the NN coordination number of approximately more than six [6]. However the local structure analyzed by a crystalline model indicated that liquid Bi and Sb are affected by Peierls distortion [40].  $S(Q, E)$  obtained by IXS shows that the excitation energy of the longitudinal acoustic mode exhibits a flat-topped dispersion curve in liquid GeTe and Bi. This unique  $Q$  dependence of the acoustic excitation energy was first predicted by a FPMD simulation on liquid Bi [41] and confirmed experimentally [39] and theoretically [42]. A FPMD simulation on liquid Sb also predicted a flat-topped dispersion curve with the bond alternation arising from Peierls distortion [43]. These results indicate that atomic dynamics in the liquids is strongly correlated with the local structure accompanying Peierls distortion.

In this paper we report IXS results on liquid  $\text{Ge}_2\text{Sb}_2\text{Te}_5$ . The longitudinal acoustic excitation energy observed in  $S(Q, E)$  exhibits a flat-topped dispersion curve as observed in liquid GeTe and liquid Bi. Furthermore, we found high energy excitation in the observed  $S(Q, E)$ , which depends on  $Q$  like an optical mode. The high excitation energy indicates that fourfold coordinated Ge atoms in liquid  $\text{Ge}_2\text{Sb}_2\text{Te}_5$  are mostly sited in the octahedral order as expected by FPMD simulations [22,25,32]. On the basis of the IXS results, we discuss atomic dynamics originating from the partial structures in liquid  $\text{Ge}_2\text{Sb}_2\text{Te}_5$ .

## II. EXPERIMENT

The IXS spectra of liquid  $\text{Ge}_2\text{Sb}_2\text{Te}_5$  were measured at the high-resolution IXS beamline (BL35XU) of SPring-8 in

Japan [44]. Backscattering at the Si (11 11 11) reflection provided a beam of approximately  $10^{10}$  photons/s in a 0.8 meV bandwidth onto the sample. The energy of the incident beam and the Bragg angle of the backscattering were 21.747 keV and approximately  $89.98^\circ$ , respectively. We used 12 spherical analyzer crystals at the end of the 10 m horizontal arm. At the beam time, however, electronic noises often appeared during temperature scans, and IXS spectra obtained by at least eight analyzers were safely available. The spectrometer resolution was approximately 1.5 meV (FWHM) depending on the analyzer crystal as measured using scattering from polymethyl methacrylate (PMMA).  $Q$  resolution  $\Delta Q$  (FWHM) was  $0.45 \text{ nm}^{-1}$  where  $Q = 4\pi E_{\text{ph}} \sin \theta_A / (hc)$  ( $E_{\text{ph}}$ ,  $\theta_A$ ,  $h$ , and  $c$  are photon energy, half of the scattering angle  $2\theta/2$  for the analyzer crystal, Planck constant, and light velocity, respectively).

As the vapor pressure of Te was very high in liquid  $\text{Ge}_2\text{Sb}_2\text{Te}_5$ , we sealed a slab of  $\text{Ge}_2\text{Sb}_2\text{Te}_5$  of 99.999% purity and 0.2 mm thickness into a sapphire cell [45]. The slab was prepared by a melt-quench method using a silica glass tube. The sample cell was placed in a chamber developed for high-pressure experiments [46] filled with He gas (99.999% purity) at 0.1 MPa to reduce the background from the air. IXS spectra of liquid  $\text{Ge}_2\text{Sb}_2\text{Te}_5$  at 943 K were measured at the scattering angles  $2\theta$  of 1.9, 4.5, 7.3, 10.1, and 12.8 deg for the analyzer platform. A scan of  $\pm 30$  meV took 2 h and 8, 10, 4, 3, and 3 scans were respectively done at  $2\theta$  values above to obtain the spectra with reasonable statistics. The background spectra were measured at 943 K and 0.1 MPa using an empty sapphire cell. After background subtraction with the absorption correction and integration with respect to  $E$ , we deduced the normalized dynamic structure factor  $S(Q, E)/S(Q)$  from the observed spectra. The integration of  $S(Q, E)$  containing the incoherent component reasonably agrees with the diffraction spectrum calculated from  $S(Q)$  of liquid  $\text{Ge}_2\text{Sb}_2\text{Te}_5$  [14] as indicated in Fig. S1 in the Supplemental Material [47].

Density measurements of liquid Te,  $\text{Sb}_2\text{Te}_3$ ,  $\text{Ge}_1\text{Sb}_2\text{Te}_4$ ,  $\text{Ge}_2\text{Sb}_2\text{Te}_5$ , GeTe were carried out by a high energy  $\gamma$ -ray attenuation method [48]. A  $^{137}\text{Cs}$  isotope and a NaI scintillation counter were used as a  $\gamma$ -ray source of 662 keV and the detector, respectively. The samples were sealed in ampoules made of fused quartz with a proper length determined by measuring the linear attenuation coefficient of Hg at room temperature. More details are described in [37].

## III. RESULTS

Figure 1 shows  $S(Q, E)/S(Q)$  of liquid  $\text{Ge}_2\text{Sb}_2\text{Te}_5$ . The spectra consist of the quasielastic component at the center and inelastic shoulders or wings on both sides.  $S(Q, E)/S(Q)$  at  $2.2 \text{ nm}^{-1}$  exhibits inelastic shoulders at approximately  $\pm 2.4$  meV. The excitation energy disperses with increasing  $Q$  and becomes approximately 15 meV at  $10.7 \text{ nm}^{-1}$ . With further increasing  $Q$ , the inelastic excitation is merged into the central peak near the  $Q$  value where  $S(Q)$  exhibits the main peak. The tails of the spectra at  $Q \leq 4.4 \text{ nm}^{-1}$  exhibit an unusual behavior. We considered that it was partly because improper background subtraction due to the acoustic phonon in sapphire. The terminations at the tails in the spectra at  $24.0$  and  $26.7 \text{ nm}^{-1}$  were caused by large inelastic excitation of sapphire phonons.

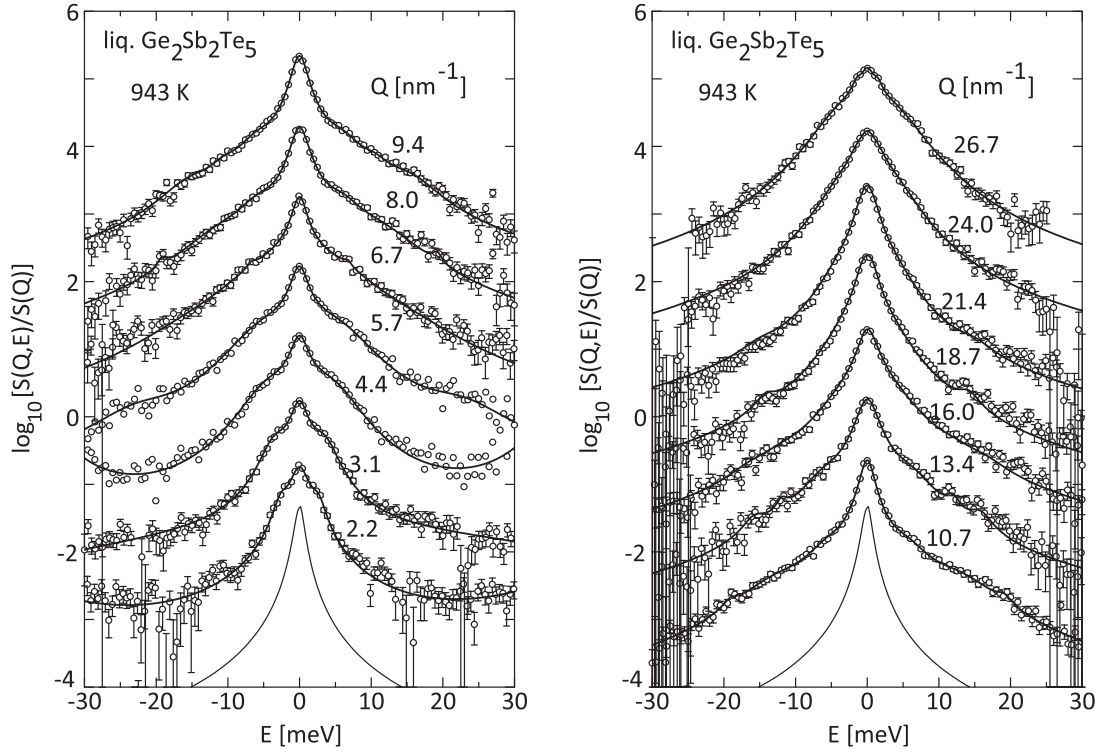


FIG. 1.  $S(Q, E)/S(Q)$  of liquid  $\text{Ge}_2\text{Sb}_2\text{Te}_5$  at 943 K and at  $Q$  denoted on the right hand side. Open circles and solid lines denote the experimental results and the optimized fits with the model function described in the text, respectively. Each spectrum is shifted by multiplying 10 and the error bars are hidden at 4.4 and 5.7  $\text{nm}^{-1}$  for clarity. The resolution function is shown by a solid line at the bottom.

To obtain the excitation energy dispersing with  $Q$ , we analyzed the experimentally obtained  $S(Q, E)/S(Q)$  using the damped harmonic oscillator (DHO) model function [49]. Such a simple model well approximated the spectra of binary liquid GeTe [38]. The model function is composed of a Lorentzian for the central peak and DHO components for the inelastic excitation,

$$F_{\text{model}}(Q, E) = \frac{A_{\text{qe}}}{\pi} \frac{\Gamma_{\text{qe}}}{\Gamma_{\text{qe}}^2 + E^2} + \sum_j \frac{a_j}{\pi} \frac{4\Omega_j\Gamma_j}{(E^2 - \omega_j^2)^2 + 4E^2\Gamma_j^2}, \quad (1)$$

where  $\Omega_j = \sqrt{\omega_j^2 - \Gamma_j^2}$  and  $a_j = k_B T A_j$ .  $A_{\text{qe}}$  and  $\Gamma_{\text{qe}}$  are the amplitude and linewidth of Lorentzian, respectively.  $A_j$ ,  $\Gamma_j$ , and  $\omega_j$  ( $j = 1, 2$ , and  $3$ ) are the amplitude, linewidth, and excitation energy of the  $j$ th inelastic excitation.  $F_{\text{model}}(Q, E)$  was convoluted using the Bose factor  $B(E) = \beta E / [1 - \exp(-\beta E)]$  where  $\beta = (k_B T)^{-1}$ , and the resolution function  $R(E)$  as

$$S(Q, E)/S(Q) = \int B(E') F_{\text{model}}(Q, E') R(E - E') dE', \quad (2)$$

and the parameters were optimized to fit the experimental  $S(Q, E)/S(Q)$  at  $|E| \leq 30$  meV. The bold curves in Fig. 1 are the best-fit results. The convoluted  $F_{\text{model}}(Q, E)$  reproduces the experimental one very well.

We applied  $j = 1$  (1-DHO),  $j = 2$  (2-DHO), and  $j = 3$  (3-DHO) models to  $S(Q, E)/S(Q)$  to investigate high energy

excitation of Ge predicted by FPMD [22,25,35,36]. As the acoustic excitation ( $\omega_1$ ) and low energy excitation ( $\omega_2$ ) were obtained in liquid GeTe [38], we assigned  $\omega_3$  to the high energy excitation. Figure 2 shows the results of these models at several  $Q$  values. Besides  $\omega_1$  and  $\omega_2$ ,  $\omega_3$  of approximately 20 meV (thin black curve) was obtained by 3-DHO at  $Q \geq 6.7 \text{ nm}^{-1}$  and 2-DHO at  $Q \leq 5.9 \text{ nm}^{-1}$ . The smaller  $\chi^2$  per degree of freedom,  $\chi^2/N$ , shown in the figure justifies the  $\omega_3$  excitation. Although the 3-DHO model did not always show the smallest  $\chi^2/N$  as indicated in the Supplemental Material [50], Bayesian analysis [51] suggested a priority of the 3-DHO model at  $12 \leq Q \leq 16 \text{ nm}^{-1}$  even if  $\chi^2/N$  values are inferior. A dispersion curve of  $\omega_1$  optimized without the  $\omega_3$  component exhibits an unusual kink at  $7 \text{ nm}^{-1}$  as shown in Fig. S2 in the Supplemental Material [52]. Considering these results, we concluded that the  $\omega_3$  mode is not artificial. Here we note that the low energy ( $\omega_2$ ) mode was not obtained in  $S(Q, E)/S(Q)$  at  $Q < 6 \text{ nm}^{-1}$  by the 2-DHO model, and that the higher excitation energy obtained by 2-DHO was assigned as  $\omega_3$ .

The  $\omega_3$  values above 30 meV were omitted in the present analysis because it was out of the surveying energy range. After these procedures, the remaining all  $\omega_1$ ,  $\omega_2$ , and  $\omega_3$  are plotted as a function of  $Q$  in Fig. S2 in the Supplemental Material [52]. Hereafter our discussion is conducted using the optimized parameters averaged at similar  $Q$ . All parameters averaged are shown in Figs. S3 and S4 in the Supplemental Material [53]. Although there might be a criticism that the present results depend on the model function, we would

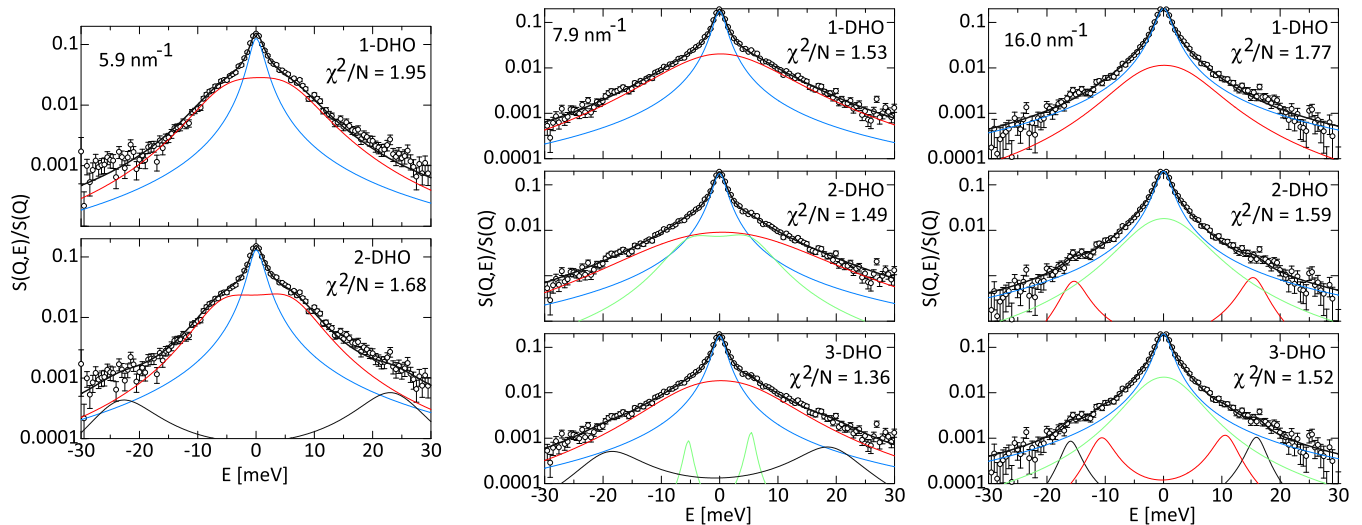


FIG. 2. The optimized fits of 1-DHO, 2-DHO, and 3-DHO models for  $S(Q, E)/S(Q)$ . A blue peak denotes the quasielastic component after convolution while red ( $\omega_1$ ), green ( $\omega_2$ ), and thin black ( $\omega_3$ ) curves denote convoluted inelastic excitations.

answer that they preserve consistency with those of liquid Bi [39] and liquid GeTe [38].

#### IV. DISCUSSION

Figure 3 shows the optimized  $\omega_1$ ,  $\omega_2$ , and  $\omega_3$  with VDOS. As shown in Fig. 3(c),  $\omega_1$  disperses linearly with increasing  $Q$  up to  $10 \text{ nm}^{-1}$  (broken line), 1.46 times faster than the ultrasonic sound speed (black line) [48]. The behavior agrees with the longitudinal acoustic excitation.  $\omega_1$  becomes approximately constant at  $12 \leq Q \leq 16 \text{ nm}^{-1}$ . The flat-topped energy of  $\omega_1$  in liquid  $\text{Ge}_2\text{Sb}_2\text{Te}_5$  approximately corresponds to the second maximum in the VDOS as shown in Fig. 3(a). The second maximum may be assigned as vibrations of Sb and Te by the VDOS simulated for liquid  $\text{Ge}_{22}\text{Sb}_{22}\text{Te}_{56}$  [36] shown in Fig. 3(b). Furthermore,  $\omega_1$  abruptly goes down at  $17 \text{ nm}^{-1}$ . The  $Q$  position is lower than the main peak one in the Sb-Te partial structure factor  $S_{\text{SbTe}}(Q)$  of liquid  $\text{Ge}_{22}\text{Sb}_{22}\text{Te}_{56}$  [36]. The main peak position is located at  $Q$  lower than that of  $S_{\text{GeTe}}(Q)$ . The consistency of  $S_{\text{SbTe}}(Q)$  and  $S_{\text{GeTe}}(Q)$  simulated is shown in Figs. S5–S7 in the Supplemental Material [54]. The fractions of the scattering cross section of Sb-Te, Te-Te, and Ge-Te correlation for x ray are approximately 0.3, 0.4, and 0.2, respectively. Although de Gennes narrowing is expected at the main peak position in a simple liquid, the case of liquid Si shows that the narrowing occurs at  $Q$  lower than the  $S(Q)$  maximum [55]. From these results, it is inferred that the flat-topped energy of  $\omega_1$  is related with the Sb-Te correlation. Here we should note that the linear dispersion at low  $Q$  should not be assigned to the partial structures [56].

The flat-topped dispersion curve has been observed in liquid Bi [39,41,42], liquid GeTe [38], and liquid Sb [43]. These liquids belong to the liquids with Peierls distortion [6,40]. In general, only one-dimensional information on structure is experimentally obtained for disordered materials. A primitive chain model applied to the flat-topped dispersion curve in liquid Bi [39] suggests that the second NN interaction was not negligible and the force constant ratio to the first NN one

was estimated approximately  $0.21 (=4.14^2 \text{ ps}^{-2}/8.98^2 \text{ ps}^{-2})$ . Such long-range interatomic force constants were reported in crystalline Bi and Sb [57]. The results suggest that intrinsic nature of the crystal brings out in the liquid state.

In addition, the effective pair potential [58] that could reproduce  $S(Q)$  in liquid Bi could not reproduce the flat-topped dispersion curve in liquid Bi (Fig. 4 in [39]) although it could reproduce a high  $Q$  part of the flat energies. The fact means that the spherical potential could not well describe the interatomic interaction in liquid Bi. As FPMD simulations [39,41–43] succeeded in reproducing the dispersion curve, it is inferred that the flat-topped dispersion curve is strongly correlated with the atomic dynamics under the force field depending on three-dimensional atomic configurations in the liquids with Peierls distortion.

Next we discuss  $\omega_2$  in Fig. 3(c). In the previous papers [38,39] we discussed its origin as the transverse acoustic mode in nonsimple liquids. The alternation of shorter and longer bonds stabilized in the liquid [21,37] may promote enhancement in a mixing of the longitudinal and transverse acoustic waves. The ratio of the maximum energy in  $\omega_2$  to that in  $\omega_1$  is approximately 1:2. It may mean that clusters composed of four atoms arising from Peierls distortion participate in the  $\omega_2$  mode through the mixing. Comparison with  $\Gamma_2$  shown in Fig. S3 in the Supplemental Material [53] indicates that the  $\omega_2$  mode is a damped one, being correlated with a short lifetime of clusters. We believe that this assignment for the  $\omega_2$  mode is correct although a heat mode was proposed in the case of a simple liquid metal by a FPMD simulation [59].

Because of a ternary liquid, another excitation besides  $\omega_1$  and  $\omega_2$  might be expected. The  $Q$  dependence of  $\omega_3$  shown in Fig. 3(c) is the most interesting in this study. It reminds us the optical mode in molten salts simulated [56]; a band crossing with the acoustic mode seems to occur approximately at  $10 \text{ nm}^{-1}$  in Fig. 3(c). The assignment of  $\omega_3$  as the optical mode, however, may be beyond the present results.

As experimental facts, the  $\omega_3$  values at  $12 \leq Q \leq 16 \text{ nm}^{-1}$  are approximately 16 meV, which is close to the flat-topped energy in liquid GeTe denoted by a chain curve. The result

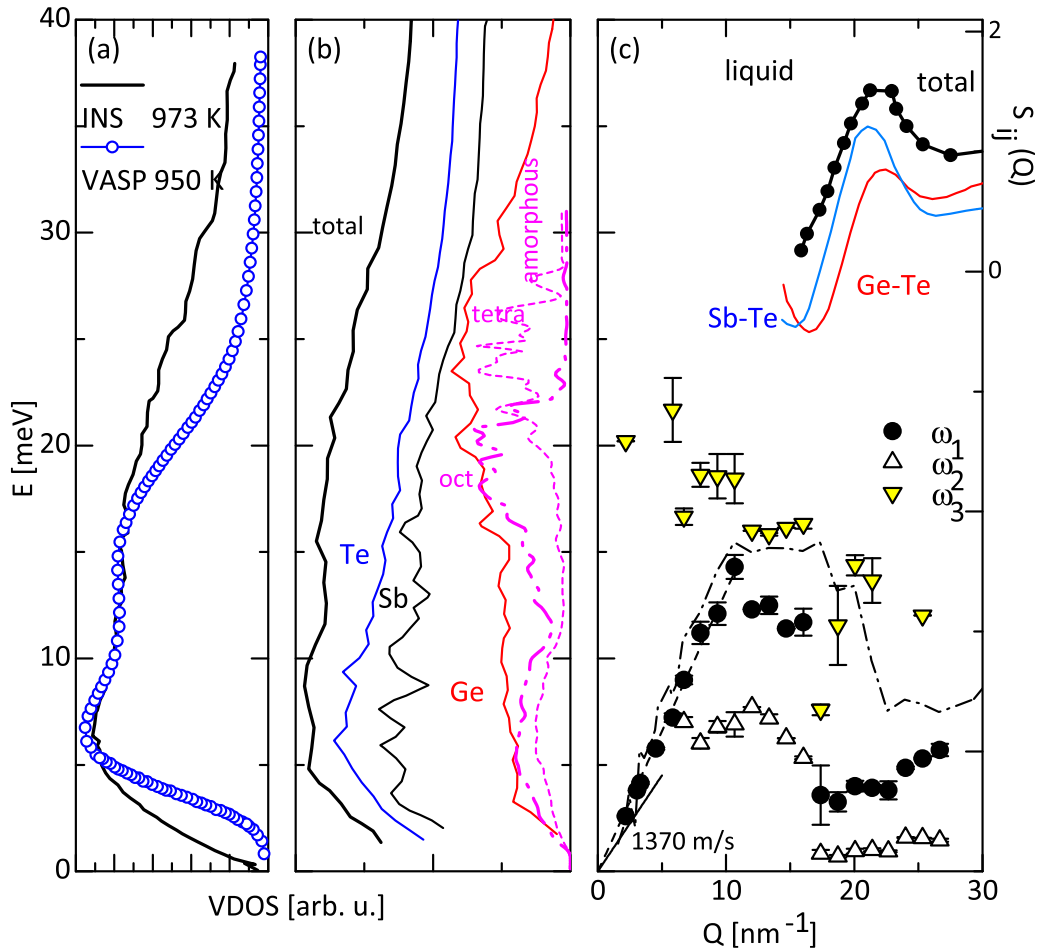


FIG. 3. (a) VDOS in liquid  $\text{Ge}_2\text{Sb}_2\text{Te}_5$  obtained by INS (black curve) and a FPMD simulation (blue circles with line) [35]. (b) VDOS in liquid  $\text{Ge}_{22}\text{Sb}_{22}\text{Te}_{56}$  obtained by a FPMD simulation [36]. Magenta curves denote VDOS of tetrahedral (broken curve) and octahedral (chain curve) Ge sites simulated for the amorphous [23]. (c)  $\omega_1$ ,  $\omega_2$ , and  $\omega_3$  in liquid  $\text{Ge}_2\text{Sb}_2\text{Te}_5$ ,  $\omega_1$  in liquid GeTe (a chain curve), and  $S(Q)$  of liquid  $\text{Ge}_2\text{Sb}_2\text{Te}_5$  (dots with line) [14], and  $S_{\text{SbTe}}(Q)$  (blue line) and  $S_{\text{GeTe}}(Q)$  (red line) of liquid  $\text{Ge}_{22}\text{Sb}_{22}\text{Te}_{56}$  [36].  $S_{\text{SbTe}}(Q)$  and  $S_{\text{GeTe}}(Q)$  are shifted by 0.5 for clarity. Also shown is the ultrasonic sound speed of liquid  $\text{Ge}_2\text{Sb}_2\text{Te}_5$  (black line).

indicates that the  $\omega_3$  mode is related with Ge-Te correlation. With decreasing  $Q$  toward  $0 \text{ nm}^{-1}$ ,  $\omega_3$  approaches approximately 20 meV, the peak energy in the Ge-VDOS shown in Fig. 3(b). Two kinds of fourfold coordinated structures around a central Ge, tetrahedral and octahedral ones, have been proposed [3]. As indicated in Table I, the fraction of

TABLE I. Fraction of Ge with tetrahedral configuration  $f_{\text{Ge-tetra}}$  in amorphous (a-) and liquid (l-)  $\text{Ge}_2\text{Sb}_2\text{Te}_5$  (GST225) and GeTe simulated by several research groups.

Simulation	System size	$T$ (K)	Sample	$f_{\text{Ge-tetra}}$
Akola and Jones [21]	460	300	a-GST225	0.34
Akola and Jones [21]	460	300	a-GeTe	0.29
Akola and Jones [22]	460	900	l-GST225	0.32
Gabardi <i>et al.</i> [24]	270	300	a-GST225	0.27
Qiao <i>et al.</i> [25]	189	1273	l-GST225	0.073
Qiao <i>et al.</i> [25]	189	300	a-GST225	0.084
Mocanu <i>et al.</i> [32]	7200	1200	l-GST225	0.01
Mocanu <i>et al.</i> [32]	7200	300	a-GST225	0.05

the octahedral Ge sites was estimated at approximately 0.7 and tetrahedral Ge sites are minor. The minor tetrahedral sites in the amorphous state are reported to decrease further with aging [60]. Although it is difficult to assign the structure from the present IXS results, the octahedral one is more plausible as the origin of  $\omega_3$  because the energy seems consistent with the vibration energy of octahedral ones (magenta chain curve) in amorphous  $\text{Ge}_2\text{Sb}_2\text{Te}_5$  predicted by FPMD simulations [22,23].

Although similarity between  $\text{Ge}_2\text{Sb}_2\text{Te}_5$  and GeTe has been predicted by FPMD simulations with respect to fourfold coordinated Ge sites as shown in Table I, the previous IXS results of liquid GeTe [38] could not give an excitation energy like  $\omega_3$ . On the other hand, VDOS simulated for amorphous GeTe exhibits vibrational components at a similar energy [61]. To investigate high energy excitation in liquid GeTe, we plot the high energy wings of  $S(Q, E)/S(Q)$  at  $5.9 \text{ nm}^{-1}$  in Fig. 4. Both liquid GeTe and  $\text{Ge}_2\text{Sb}_2\text{Te}_5$  seem to exhibit a broad hump at approximately 22 meV especially in negative  $E$  region, but the signal to noise ratio in liquid GeTe was much worse than in liquid  $\text{Ge}_2\text{Sb}_2\text{Te}_5$ . Hence fits with 1-DHO and

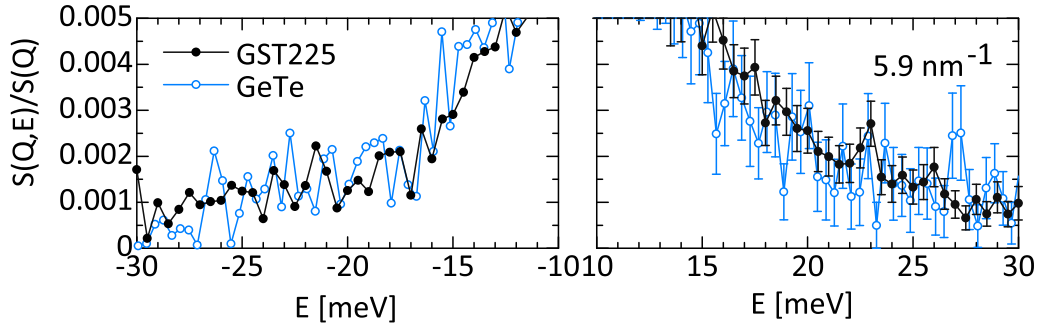


FIG. 4. High energy wings in  $S(Q, E)/S(Q)$  of liquid  $\text{Ge}_2\text{Sb}_2\text{Te}_5$  and GeTe. Error bars in the negative  $E$  range are not displayed for clarity.

2-DHO models did not give large  $\chi^2/N$  values or fluctuations in the optimized energy in the case of liquid GeTe. As a result, we could not be aware of a possibility of  $\omega_3$  in liquid GeTe.

The transformation into the metastable rocksalt structure in PCMs has been considered to be an important property with respect to fast crystallization [10]. As the metastable rocksalt structure has vacancies at cation sites in  $\text{Ge}_2\text{Sb}_2\text{Te}_5$ , the source of vacancies may arise from cavities in the liquid phase. In fact, FPMD simulations on the liquid and amorphous [21,22] indicated that the vacancy concentration is larger in  $\text{Ge}_2\text{Sb}_2\text{Te}_5$  than in GeTe and that vacancies are distributed around Te atoms. Figure 5 shows the molar volume  $V_M$  experimentally determined at 1073 K in Ge-Sb-Te ternary liquids including GeTe and  $\text{Sb}_2\text{Te}_3$  [48]. Also shown is  $V_M$  calculated from  $V_M$  of each elemental liquid (see Table II). Experimental and calculated  $V_M$ 's agree with each other like an ideal liquid, not only in the ternary liquids but also in the binary ones. This fact means that no excess volume for vacancies appears when Sb atoms with large  $V_M$  are substituted into liquid GeTe as far as each atom shares its own volume. From FPMD simulations on liquid Sb [43] and liquid Te [63], however, cavities were predicted in these monatomic liquids. Because cavities in liquid Te are common in these mixtures, several % cavity volumes in liquid Sb will act as a source of vacancies in liquid  $\text{Ge}_2\text{Sb}_2\text{Te}_5$ .

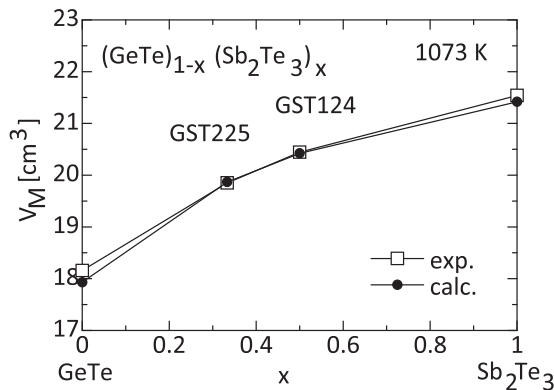


FIG. 5. Molar volume  $V_M$  of liquid  $(\text{GeTe})_{1-x}(\text{Sb}_2\text{Te}_3)_x$  at 1073 K. GST225 and GST124 denote  $\text{Ge}_2\text{Sb}_2\text{Te}_5$  and  $\text{Ge}_1\text{Sb}_2\text{Te}_4$ , respectively.  $V_M$  experimentally determined and that calculated using elemental values are indicated by open squares and black circles, respectively.

Previously it was discussed that negative thermal expansion in a liquid Ge-Te alloy is in the counterrelationship with Peierls distortion [6,35]. In the present temperature range, however, liquid GeTe and  $\text{Ge}_2\text{Sb}_2\text{Te}_5$  show normal thermal expansion, with Peierls distortion smeared out with increasing temperature. Here we compare the molar volume per valence electron  $V_M/n_{\text{val}}$  in Table II.  $V_M/n_{\text{val}}$  becomes large with increasing Sb concentration in order of GeTe,  $\text{Ge}_2\text{Sb}_2\text{Te}_5$ , and  $\text{Ge}_1\text{Sb}_2\text{Te}_4$ . Despite that the valence electron number increases from GeTe to  $\text{Ge}_2\text{Sb}_2\text{Te}_5$ , the  $V_M$  is expanded much more with the Sb substitution. The result implies that Peierls distortion is weakened with the substitution of Sb into GeTe. This effect is inferred to be correlated with stability of the rocksalt structure at the room temperature in  $\text{Ge}_2\text{Sb}_2\text{Te}_5$ .

Finally, we discuss the quasielastic component in  $S(Q, E)/S(Q)$ . Figure 6 shows  $\Gamma_{\text{eq}}$  of liquid  $\text{Ge}_2\text{Sb}_2\text{Te}_5$  and GeTe as a function of  $Q$ . As discussed in [38], the narrowing of  $\Gamma_{\text{eq}}$  in liquid GeTe is correlated with  $S_{\text{TeTe}}(Q)$  in the liquid. The result suggests that the diffusion coefficient of Te is smaller than that of Ge in liquid GeTe. Meanwhile,  $\Gamma_{\text{eq}}$  in liquid  $\text{Ge}_2\text{Sb}_2\text{Te}_5$  becomes narrow in a wider  $Q$  range from 17 to 26  $\text{nm}^{-1}$ , whereas  $S_{\text{TeTe}}(Q)$  exhibits a maximum at 20  $\text{nm}^{-1}$ . As shown in Fig. S6 in the Supplemental Material [54], the maxima of  $S_{ij}(Q)$  in liquid  $\text{Ge}_2\text{Sb}_2\text{Te}_5$  are located from 17 to 24  $\text{nm}^{-1}$ . These results indicate that all elements in liquid  $\text{Ge}_2\text{Sb}_2\text{Te}_5$  are equally not diffusive. We could not conclude that lighter Ge atoms are more diffusive because diffusion coefficients of Ge depend on the simulations [21,25,65]. The

TABLE II. Molar volume  $V_M$  experimentally obtained at 1073 K and  $V_{M,\text{calc.}}$  calculated from elemental  $V_M$  experimentally obtained at 1073 K (listed below). Here  $V_M$  of Ge is linearly extrapolated to the undercooled liquid state. Also shown are the number of valence electrons per atom  $n_{\text{val}}$  and the molar volume per valence electron  $V_M/n_{\text{val}}$ .

Sample	$n_{\text{val}}$	$V_M$ (cm <sup>3</sup> )	$V_{M,\text{calc.}}$ (cm <sup>3</sup> )	$V_M/n_{\text{val}}$ (cm <sup>3</sup> )
GeTe [48]	5	18.16	17.93	3.63
$\text{Ge}_2\text{Sb}_2\text{Te}_5$ [48]	5.33	19.85	19.87	3.72
$\text{Ge}_1\text{Sb}_2\text{Te}_4$ [48]	5.43	20.44	20.42	3.77
$\text{Sb}_2\text{Te}_3$ [48]	5.6	21.54	21.42	3.85
Ge [62]	4	12.87		3.22
Sb [62]	5	19.06		3.81
Te [48]	6	22.99		3.83

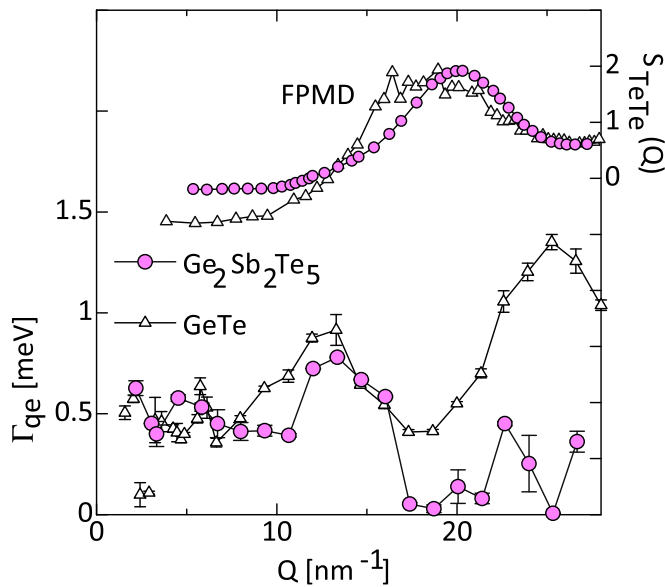


FIG. 6. The quasielastic linewidth  $\Gamma_{qe}$  of liquid  $\text{Ge}_2\text{Sb}_2\text{Te}_5$  (magenta circles) and  $\text{GeTe}$  (open triangles), with  $S_{\text{TeTe}}(Q)$  obtained by FPMD simulations on liquid  $\text{Ge}_{22}\text{Sb}_{22}\text{Te}_{56}$  [36] and liquid  $\text{GeTe}$  [64].

results imply that Ge, Sb, and Te atoms equally contributed to atomic dynamics in the liquid as commented on fast crystallization from an undercooled liquid phase in [31].

## V. SUMMARY

The present IXS investigation revealed that the dynamic structure factor in liquid  $\text{Ge}_2\text{Sb}_2\text{Te}_5$  exhibits a flat-topped dispersion curve that is split into higher and lower energies arising from Ge-Te and Sb-Te correlations, respectively. The high energy excitation behaves like an optical mode, approaching higher energy corresponding to the vibrational energy of fourfold coordinated Ge with octahedral order. The low energy excitation is assigned to the transverse acoustic excitation in liquid  $\text{Ge}_2\text{Sb}_2\text{Te}_5$  as well as in liquid  $\text{GeTe}$ . From the molar volume experimentally obtained, we found a possibility that the weakening of Peierls distortion in liquid  $\text{Ge}_2\text{Sb}_2\text{Te}_5$  compared to liquid  $\text{GeTe}$  is correlated with the stability of metastable rocksalt structure at the room temperature.

## ACKNOWLEDGMENTS

We would like to thank Dr. Shinji Kohara, Professor Robert O. Jones, and Professor Jaakko Akola for their valuable discussion. The authors acknowledge Ministry of Education, Culture, Sports, Science and Technology in Japan and the Japan Society for the Promotion of Science (JSPS) for a Grant-in-Aid for Scientific Research (A) (Grant No. 20244061) and Scientific Research (B) (Grant No. 16340114). The synchrotron radiation experiments were performed at the SPring-8 with the approval of the Japan Synchrotron Radiation Research Institute (JASRI) (Proposals No. 2019A1195, No. 2018B1221, and No. 2013B1269).

- [1] S. R. Ovshinsky, *Phys. Rev. Lett.* **21**, 1450 (1968).
- [2] K. Shportko, S. Kremers, M. Woda, D. Lencer, J. Robertson, and M. Wuttig, *Nat. Mater.* **7**, 653 (2008).
- [3] B. Huang and J. Robertson, *Phys. Rev. B* **81**, 081204(R) (2010).
- [4] M. Wuttig, V. L. Deringer, X. Gonze, C. Bichara, and J.-Y. Raty, *Adv. Mater.* **30**, 1803777 (2018).
- [5] B. J. Kooi and M. Wuttig, *Adv. Mater.* **32**, 1908302 (2020).
- [6] J.-P. Gaspard, *C. R. Phys.* **17**, 389 (2016).
- [7] S. Maier, S. Steinberg, Y. Cheng, C.-F. Schön, M. Schumacher, R. Mazzarello, P. Golub, R. Nelson, O. Cojocaru-Mirédin, J.-Y. Raty, and M. Wuttig, *Adv. Mater.* **32**, 2005533 (2020).
- [8] R. E. Peierls, *Quantum Theory of Solids* (Oxford University Press, Oxford, 1955).
- [9] H. Jones, *Proc. R. Soc. London Ser. A* **147**, 396 (1934).
- [10] R. O. Jones, *Phys. Rev. B* **101**, 024103 (2020).
- [11] R. Bellissent, C. Bergman, R. Ceolin, and J. P. Gaspard, *Phys. Rev. Lett.* **59**, 661 (1987).
- [12] M. Delheusy, J. Y. Raty, R. Detemple, W. Welnic, M. Wuttig, and J.-P. Gaspard, *Physica B* **350**, e1055 (2004).
- [13] C. Steimer, V. Coulet, W. Welnic, H. Dieker, R. Detemple, C. Bichara, B. Beuneu, J.-P. Gaspard, and M. Wuttig, *Adv. Mater.* **20**, 4535 (2008).
- [14] S. Kohara, K. Kato, S. Kimura, H. Tanaka, T. Usuki, K. Suzuya, H. Tanaka, Y. Moritomo, T. Matsunaga, N. Yamada, Y. Tanaka, H. Suematsu, and M. Takata, *Appl. Phys. Lett.* **89**, 201910 (2006).
- [15] P. Jónvári, I. Kaban, J. Steiner, B. Beuneu, A. Schöps, and M. A. Webb, *Phys. Rev. B* **77**, 035202 (2008).
- [16] S. Hosokawa, W.-C. Pilgrim, A. Höhle, D. Szubrin, N. Boudet, J.-F. Beřar, and K. Maruyama, *J. Appl. Phys.* **111**, 083517 (2012).
- [17] K. Ohara, L. Temleitner, K. Sugimoto, S. Kohara, T. Matsunaga, L. Pusztai, M. Itou, H. Ohsumi, R. Kojima, N. Yamada, T. Usuki, A. Fujiwara, and M. Takata, *Adv. Funct. Mater.* **22**, 2251 (2012).
- [18] J. R. Stellhorn, S. Hosokawa, B. Kaiser, K. Kimura, N. Boudet, N. Blanc, H. Tajiri, S. Kohara, and W.-C. Pilgrim, *Z. Phys. Chem.* **235**, 141 (2021).
- [19] E. Matsubara, S. Okada, T. Ichitsubo, T. Kawaguchi, A. Hirata, P. F. Guan, K. Tokuda, K. Tanimura, T. Matsunaga, M. W. Chen, and N. Yamada, *Phys. Rev. Lett.* **117**, 135501 (2016).
- [20] A. Hirata, T. Ichitsubo, P. F. Guan, T. Fujita, and M. W. Chen, *Phys. Rev. Lett.* **120**, 205502 (2018).
- [21] J. Akola and R. O. Jones, *Phys. Rev. B* **76**, 235201 (2007).
- [22] J. Akola and R. O. Jones, *J. Phys.: Condens. Matter* **20**, 465103 (2008).
- [23] S. Caravati, M. Bernasconi, T. D. Kühne, M. Krack, and M. Parrinello, *J. Phys.: Condens. Matter* **21**, 255501 (2009).
- [24] S. Gabardi, S. Caravati, M. Bernasconi, and M. Parrinello, *J. Phys.: Condens. Matter* **24**, 385803 (2012).
- [25] C. Qiao, Y. R. Guo, F. Dong, J. J. Wang, H. Shen, S. Y. Wang, M. Xu, X. S. Miao, Y. X. Zheng, R. J. Zhang, L. Y. Chen, C. Z. Wang, and K. M. Ho, *J. Mater. Chem. C* **6**, 5001 (2018).
- [26] J. Orava, A. L. Greer, B. Gholipour, D. W. Hewak, and C. E. Smith, *Nat. Mater.* **11**, 279 (2012).
- [27] T. H. Lee and S. R. Elliott, *Adv. Mater.* **29**, 1700814 (2017).

- [28] J. Hegedüs and S. R. Elliott, *Nat. Mater.* **7**, 399 (2008).
- [29] J. Kalikka, J. Akola, J. Larrucea, and R. O. Jones, *Phys. Rev. B* **86**, 144113 (2012).
- [30] J. Kalikka, J. Akola, and R. O. Jones, *Phys. Rev. B* **90**, 184109 (2014).
- [31] J. Kalikka, J. Akola, and R. O. Jones, *Phys. Rev. B* **94**, 134105 (2016).
- [32] F. C. Mocanu, K. Konstantinou, T. H. Lee, N. Bernstein, V. L. Deringer, G. Csányi, and S. R. Elliott, *J. Phys. Chem. B* **122**, 8998 (2018).
- [33] N. Yamada and T. Matsunaga, *J. Appl. Phys.* **88**, 7020 (2000).
- [34] A. V. Kolobov, P. Fons, M. Krbal, R. E. Simpson, S. Hosokawa, T. Uruga, H. Tanida, and J. Tominaga, *Appl. Phys. Lett.* **95**, 241902 (2009).
- [35] C. Otjacques, J.-Y. Raty, M.-V. Coulet, M. Johnson, H. Schober, C. Bichara, and J.-P. Gaspard, *Phys. Rev. Lett* **103**, 245901 (2009).
- [36] H. Flores-Ruiz, M. Micoulaut, M.-V. Coulet, A. A. Piarristeguy, M. R. Johnson, G. J. Cuello, and A. Pradel, *Phys. Rev. B* **92**, 134205 (2015).
- [37] M. Schumacher, H. Weber, P. Jónvári, Y. Tsuchiya, T. G. A. Youngs, I. Kaban, and R. Mazzarello, *Sci. Rep.* **6**, 27434 (2016).
- [38] M. Inui, A. Koura, Y. Kajihara, S. Hosokawa, A. Chiba, K. Kimura, F. Shimojo, S. Tsutsui, and A. Q. R. Baron, *Phys. Rev. B* **97**, 174203 (2018).
- [39] M. Inui, Y. Kajihara, S. Munejiri, S. Hosokawa, A. Chiba, K. Ohara, S. Tsutsui, and A. Q. R. Baron, *Phys. Rev. B* **92**, 054206 (2015).
- [40] M. Mayo, E. Yahel, Y. Greenberg, and G. Makov, *J. Phys: Condens. Matter* **25**, 505102 (2013).
- [41] J. Souto, M. M. G. Alemany, L. J. Gallego, L. E. González, and D. J. González, *Phys. Rev. B* **81**, 134201 (2010).
- [42] M. Ropo, J. Akola, and R. O. Jones, *J. Chem. Phys.* **145**, 184502 (2016).
- [43] R. O. Jones, O. Ahlstedt, J. Akola, and M. Ropo, *J. Chem. Phys.* **146**, 194502 (2017).
- [44] A. Q. R. Baron, Y. Tanaka, S. Goto, K. Takeshita, T. Matsushita, and T. Ishikawa, *J. Phys. Chem. Solids* **61**, 461 (2000).
- [45] K. Tamura, M. Inui, and S. Hosokawa, *Rev. Sci. Instrum.* **70**, 144 (1999).
- [46] S. Hosokawa and W.-C. Pilgrim, *Rev. Sci. Instrum.* **72**, 1721 (2001).
- [47] See Supplemental Material at <http://link.aps.org/supplemental/10.1103/PhysRevB.104.064202> for comparison of the  $E$  integration of  $S(Q, E)$  with  $F(Q)$  calculated using  $S(Q)$  experimentally obtained [14].
- [48] C. Otjacques, J.-Y. Raty, J.-P. Gaspard, Y. Tsuchiya, and C. Bichara, *Collection SFN* **12**, 233 (2011).
- [49] B. Fåk and B. Dorner, *Physica B* **234–236**, 1107 (1997).
- [50] See Supplemental Material at <http://link.aps.org/supplemental/10.1103/PhysRevB.104.064202> for the optimized fits shown in Figs. S8–S23.
- [51] D. S. Sivia and J. Skilling, *Data Analysis, A Bayesian Tutorial, 2nd ed.* (Oxford University Press, Oxford, UK, 2006).
- [52] See Supplemental Material at <http://link.aps.org/supplemental/10.1103/PhysRevB.104.064202> for the optimized  $\omega_1$ ,  $\omega_2$ , and  $\omega_3$ , and a dispersion curve of the longitudinal acoustic mode that we obtained, not taking account of the higher-energy excitation.
- [53] See Supplemental Material at <http://link.aps.org/supplemental/10.1103/PhysRevB.104.064202> for the optimized parameters,  $A_j$ ,  $\Gamma_j$ ,  $A_{qe}$ , and  $\Gamma_{qe}$  averaged at each  $Q$  value.
- [54] See Supplemental Material at <http://link.aps.org/supplemental/10.1103/PhysRevB.104.064202> for the partial pair distribution functions  $g_{ij}(r)$  and partial structure factors  $S_{ij}(Q)$  obtained by FPMD simulations [22,36,37].
- [55] S. Hosokawa, W.-C. Pilgrim, Y. Kawakita, K. Ohshima, S. Takeda, D. Ishikawa, S. Tsutsui, Y. Tanaka, and A. Q. R. Baron, *J. Phys.: Condens. Matter* **15**, L623 (2003).
- [56] T. Bryk and I. Mryglod, *Phys. Rev. B* **71**, 132202 (2005).
- [57] S. Lee, K. Esfarjani, T. Luo, J. Zhou, Z. Tian, and G. Chen, *Nat. Commun.* **5**, 3525 (2014).
- [58] M. Dzugutov and U. Dahlborg, *Phys. Rev. A* **40**, 4103 (1989).
- [59] T. Bryk and J.-F. Wax, *J. Chem. Phys.* **144**, 194501 (2016).
- [60] J. Y. Raty, W. Zhang, J. Luckas, C. Chen, R. Mazzarello, C. Bichara, and M. Wuttig, *Nat. Commun.* **6**, 7467 (2015).
- [61] J.-Y. Raty, P. Noé, G. Ghezzi, S. Maîtrejean, C. Bichara, and F. Hippert, *Phys. Rev. B* **88**, 014203 (2013).
- [62] *Revised 4th Edition Kinzoku (Metal) Data Book* in Japanese, edited by Japan Inst. of Metals and Materials (Maruzen Pub. 2004).
- [63] J. Akola, R. O. Jones, S. Kohara, T. Usuki, and E. Bychkov, *Phys. Rev. B* **81**, 094202 (2010).
- [64] A. Koura and F. Shimojo, *EPJ Web Conf.* **151**, 01002 (2017).
- [65] F.-C. Pang, D. Wang, N.-K. Chen, S.-Y. Xie, X. Meng, C.-S. Huo, H. Yang, X.-P. Su, W.-Q. Wang, and H.-L. Tu, *Comput. Mater. Sci.* **61**, 287 (2012).